Journal of The Electrochemical Society, **147** (8) 2930-2940 (2000)
S0013-4651(99)12-086-X CCC: $7.00

The Impedance Response of a Porous Electrode Composed of Intercalation Particles

Jeremy P. Meyers,[a,*,c,z] Marc Doyle,[b,*] Robert M. Darling,[a,*,d] and John Newman[a,]**

[a]*Department of Chemical Engineering, University of California, Berkeley, California 94720-14962, USA*
[b]*DuPont Central Research and Development, Experimental Station, Wilmington, Delaware 19880-0262, USA*

A mathematical model is developed to describe the impedance response of a porous electrode composed of spherical intercalation particles. The model considers a porous electrode without solution-phase diffusion limitations. The model is developed by first deriving the impedance response of a single intercalation particle, obtained by solving a set of governing equations which describe charge-transfer and double-layer charging at the surface, solid-phase diffusion inside the particle, and an open-circuit potential which varies as a function of intercalant concentration. The model also considers the effect of an insulating film surrounding the particle. The governing equations are linearized to take advantage of the small amplitude of the perturbing current in impedance analysis. Once the impedance of a single particle is determined, this result is incorporated into a model which describes a porous electrode limited by ohmic drop in the solution and solid phases, and by the impedance of the particles of which the porous electrode is composed. The model can be used to examine the effect of physical properties and particle-size distributions in the porous electrode, and the usefulness of impedance analysis to measure solid-phase diffusion coefficients is scrutinized.

Manuscript submitted December 23, 1999; revised manuscript received May 19, 2000.

Electrochemical impedance spectroscopy (EIS) is a technique consisting of the application of a small perturbing current or voltage to an electrochemical system and measuring the response of the system. The response of the system can be described as an impedance, *Z*, which is the ratio, or transfer function, of the voltage to the current. Because the perturbation is small, the response of the system is linear, and the same transfer function should result whether the applied signal is a potential difference or a current. Because some processes are related to the time derivatives of potential and concentration rather than upon the magnitude of the variables themselves, some part of the system response will be in-phase with the perturbation (a real component), and some part will be out-of-phase with the applied signal (an imaginary component). The designations "real" and "imaginary" come from the mathematical notation of writing a periodic signal with frequency ω as the magnitude of the signal multiplied by the real part of the exponential of $j\omega t$.

The impedance responses of electrochemical systems have been described in the past as an arrangement of ideal equivalent-circuit elements. Simple lumped-parameter circuits and more complex finite-transmission-line circuits have been used in the past, but the disadvantage of this approach is the difficulty in interpreting the equivalent-circuit parameters in terms of fundamental properties. In this paper, the impedance is determined by describing mathematically the fundamental physical processes which govern the response of the system. This approach has been taken for many electrochemical systems to describe the impedance response.[1-5] This phenomenological approach to modeling is taken in this paper and combined with porous electrode theory[6-8] to describe the impedance of an electrode composed of spherical intercalation particles, where the interfacial processes and ohmic drop in the electrode act to distribute the reaction rate throughout the depth of the electrode.

By describing the impedance of a single intercalation particle as a function of frequency, one can gain insight into the interpretation of EIS experiments for the measurement of fundamental physical properties, and the impedance of a single particle can be incorporated into a model which describes the response of an entire porous electrode and an entire battery system. This will aid in the evaluation of results of EIS experiments as a diagnostic technique for the development of novel batteries.

* Electrochemical Society Active Member.
** Electrochemical Society Fellow.
[c] Current address: Bell Laboratories, Murray Hill, New Jersey 07974, USA.
[d] Current address: General Motors Global Alternative Propulsion Center, Honeoye Falls, New York 14472, USA.
[z] E-mail: meyers@stanfordalumni.org

Mathematical Model

We describe the impedance response of a system by solving the governing equations subject to the condition that the current is a sinusoidally varying signal with frequency ω and amplitude *I*. Each variable which is relevant to the description of the system can be resolved into a term which corresponds to the dc response of the system and another term which is governed by the perturbing signal. For a system variable *X*, one can write

$$X = X\big|_{\mathrm{DC}} + Re[\tilde{X}e^{j\omega t}] \qquad [1]$$

where $X\big|_{\mathrm{DC}}$ is the value of *X* evaluated under steady-state conditions in the absence of a perturbing signal. The perturbation is small enough that the response of the system can be considered linear. Higher-order terms are neglected

$$f(X) = f(X\big|_{\mathrm{DC}} + Re[\tilde{X}e^{j\omega t}]) = f(X\big|_{\mathrm{DC}}) + \left.\frac{df}{dX}\right|_{\mathrm{DC}} Re[\tilde{X}e^{j\omega t}] \qquad [2]$$

For perturbations about a steady state at open circuit, one can neglect the time variation of the dc component and write

$$\frac{\partial X}{\partial t} = Re[j\omega\tilde{X}e^{j\omega t}] \qquad [3]$$

A diagram of the system under consideration is shown in Fig. 1. A spherical particle is surrounded by a resistive film. One must consider charge transfer and double-layer charging across each interface, as well as the possibility of ohmic film resistance and separation of charge across the film.

At any interface, the faradaic current density is related to the potential drop across the interface by the Butler-Volmer equation

$$i_{n,\mathrm{faradaic}} = i_0\left(\exp\left[\frac{\alpha_a F}{RT}(\Phi_1 - \Phi_2 - U)\right] - \exp\left[\frac{-\alpha_c F}{RT}(\Phi_1 - \Phi_2 - U)\right]\right) \qquad [4]$$

This equation is applied at each interface; in this formulation, Φ_1 refers to the potential in the phase which is closest to the electronic conductor and Φ_2 refers to the potential in the phase which is closest to the ionic conductor. *U* is the open-circuit potential (OCP) of the charge-transfer reaction. It is the value of the potential difference

S0013-4651(99)12-086-X CCC: $7.00

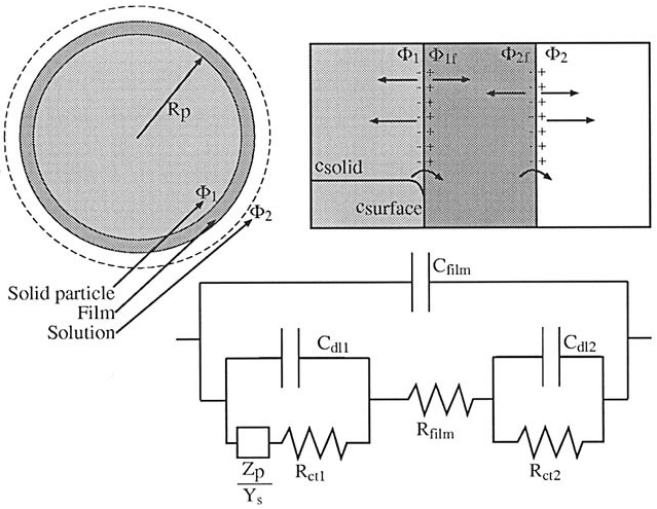

Figure 1. Schematic diagram of intercalation particle, with a detailed picture of the particle-film and film-solution interface and an equivalent-circuit diagram of the interfaces.

$\Phi_1 - \Phi_2$ when the reaction is equilibrated. The term in parentheses, $(\Phi_1 - \Phi_2 - U)$, is a surface overpotential and quantifies the degree to which the interface is removed from equilibrium. The constant i_0, the exchange current density, is a kinetic constant which determines the rate of the reaction when the system is removed from equilibrium. Strictly speaking, this constant depends upon local concentrations at the interface. If the system is being perturbed about equilibrium conditions, however, the exponential terms sum to zero, and the change in the value of the exchange current density with local concentrations does not matter, since the perturbation in this quantity is multiplied by a term which sums to zero.

There is also a current density which develops from the charging and discharging of the electrochemical double layer at the interface surrounding each particle

$$i_{n,\mathrm{dl}} = \frac{\partial q}{\partial t} = C_{\mathrm{dl}} \frac{\partial(\Phi_1 - \Phi_2)}{\partial t} \qquad [5]$$

These faradaic and nonfaradaic current densities can be added together to yield the total current density crossing the interface. These current densities are considered to be additive and to have no effect on one another, as was first posed by Grahame in his work[9]

$$i_{n,\mathrm{interface}} = i_{n,\mathrm{faradaic}} + i_{n,\mathrm{dl}} \qquad [6]$$

With the presence of an insulating film surrounding the particle, we allow for a resistive current density across the film

$$\Phi_{1\mathrm{f}} - \Phi_{2\mathrm{f}} = i_{n,\mathrm{film}} R_{\mathrm{film}} \qquad [7]$$

where the subscript f indicates that the quantity described is the value of the quantity in the film at the numbered interface.

For the separation of charge across the dielectric of the film

$$i_{\mathrm{dl,film}} = C_{\mathrm{film}} \frac{\partial(\Phi_{1\mathrm{f}} - \Phi_{2\mathrm{f}})}{\partial t} \qquad [8]$$

The capacity of the film is described by a simple dielectric

$$C_{\mathrm{film}} \frac{\epsilon}{h_{\mathrm{film}}} \qquad [9]$$

where ϵ is the permittivity of the film and h_{film} is the thickness of the film. The capacity of the film is probably very small, but if the film is a dielectric, it is possible to separate charge across it. Only at very high frequency will there be significant current flowing due to separation of charges across the film, resulting in "shorting" of the resistance of the film.

The total outward normal current density is equal to the sum of these partial current densities

$$i_n = i_{n,\mathrm{film}} + i_{\mathrm{dl,film}} \qquad [10]$$

Solid-phase diffusion and capacity limitations.—Transfer function between faradaic current and surface concentration.—The impedance response of a simple particle, such as a metal whose composition does not change with the passage of current, is sufficiently described in the previous section. If, however, there is a change in the OCP, U, as a function of the intercalant concentration in the particle, then one must perform a mass balance to determined the concentration of material in the particle, in order to determine how the OCP varies with the passage of current.

The diffusion of species in the particle is assumed to obey Fick's law. This can be shown to be valid even if the mobile intercalant species is charged, provided that the electronic mobility is much greater than that of the intercalant species

$$N_{\mathrm{intercalant}} = -D_{\mathrm{s}} \nabla c_{\mathrm{s}} \qquad [11]$$

where $N_{\mathrm{intercalant}}$ is the flux of the intercalant species, D_{s} is the diffusion coefficient of the intercalant in the particle, and c_{s} is its concentration. This expression for the flux yields the material balance in spherical coordinates

$$\frac{\partial c_{\mathrm{s}}}{\partial t} = \frac{D_{\mathrm{s}}}{r^2} \frac{\partial}{\partial r}\left(r^2 \frac{\partial c_{\mathrm{s}}}{\partial r} \right) \qquad [12]$$

where r is the radial position in the spherical particle. We can also relate the concentration gradient at the particle's surface to the interfacial faradaic current density

$$N_{\mathrm{intercalant}} = \frac{i_{n,\mathrm{faradaic}}}{F} = -D_{\mathrm{s}} \frac{\partial c_{\mathrm{s}}}{\partial \mathrm{r}}\bigg|_{\mathrm{r}=R_{\mathrm{s}}} \qquad [13]$$

That is, the flux of intercalant out of the particle is related to the faradaic current density by Faraday's law. Note that only the faradaic component of the total interfacial current density is related to a concentration gradient in the solid particle, because no intercalation material crosses the interface for current density due to double-layer charging. Strictly speaking, the charge in the double layer is due to surface excess charge, which may be due to both intercalant and the electronics in the solid, but it is assumed here that the excess charge in the double layer is due to electrons only.

Let us consider the concentration change in the solid intercalant particle as a function of the perturbing signal and frequency. Equation 12 can be rewritten for perturbations from a steady-state value

$$j\omega \tilde{c}_{\mathrm{s}} = \frac{D_{\mathrm{s}}}{r^2} \frac{\partial}{\partial r}\left(r^2 \frac{\partial \tilde{c}_{\mathrm{s}}}{\partial r} \right) \qquad [14]$$

This differential equation has the solution

$$\tilde{c}_{\mathrm{s}} = \frac{\tilde{i}_{n,\mathrm{faradaic}}}{F}\left(\frac{R_{\mathrm{s}}}{D_{\mathrm{s}}}\right)\left(\frac{1}{\sinh\left(\sqrt{j\,\Omega_{\mathrm{s}}}\right) - \sqrt{j\,\Omega_{\mathrm{s}}}\,\cosh\sqrt{j\,\Omega_{\mathrm{s}}}}\right) \frac{\sinh\left(\rho\sqrt{j\,\Omega_{\mathrm{s}}}\right)}{\rho} \qquad [15]$$

where $\rho = r/R_{\mathrm{s}}$ an $\Omega_{\mathrm{s}} = \omega R_{\mathrm{s}}^2/D_{\mathrm{s}}$.

The OCP of the intercalation reaction depends upon the concentration of intercalant at the surface of the particle. For convenience, we define $\tilde{c}_{\mathrm{surface}}$, the concentration of intercalant at the surface of the particle

$$\tilde{c}_{\mathrm{surface}} \equiv \tilde{c}_{\mathrm{s}}|_{\mathrm{r}=R} \qquad [16]$$

Then the surface concentration is related to the interfacial faradaic current density

S0013-4651(99)12-086-X CCC: $7.00

$$\tilde{c}_{\text{surface}} = \frac{\tilde{i}_{n,\text{faradaic}}}{F}\frac{R_s}{D_s}\frac{\sinh\left(\sqrt{j\Omega_s}\right)}{\sinh\left(\sqrt{j\Omega_s}\right) - \left[\sqrt{j\Omega_s}\right]\cosh\left(\sqrt{j\Omega_s}\right)} \quad [17]$$

We define the dimensionless transfer function Y_s

$$Y_s = -\frac{\tilde{i}_{n,\text{faradaic}}R_s}{FD_s\tilde{c}_{\text{surface}}} = \frac{\sqrt{j\Omega_s} - \tanh\sqrt{j\Omega_s}}{\tanh\left(\sqrt{j\Omega_s}\right)} \quad [18]$$

Change in OCP with passage of current.—The transfer function relating the concentration perturbation to the magnitude of the faradaic current density can now be incorporated into the Butler-Volmer equation to determine the impedance of the faradaic reaction at the particle/film interface. Linearization of the Butler-Volmer equation about open-circuit conditions gives

$$\tilde{i}_{n,\text{faradaic}} = \frac{i_{0,1}(\alpha_a + \alpha_c)F}{RT}\left[\tilde{\Phi}_1 + \tilde{\Phi}_{1f} - \left(-\frac{\partial U}{\partial c_s}\right)\tilde{c}_{\text{surface}}\right] \quad [19]$$

$$= \frac{i_{0,1}(\alpha_a + \alpha_c)F}{RT}\left[\tilde{\Phi}_1 - \tilde{\Phi}_{1f} - \left(-\frac{\partial U}{\partial c_s}\right)\frac{R_s}{FD_sY_s}\tilde{i}_{n,\text{faradaic}}\right]$$

The following definitions

$$R_{ct,1} = \frac{RT}{i_{0,1}(\alpha_a + \alpha_c)F}$$
$$R_{\text{part}} = \left(-\frac{\partial U}{\partial c_s}\right)\frac{R_s}{FD_s} \quad [20]$$

allows us to write the relationship between the faradaic current density and the potential across the interface as

$$\tilde{i}_{n,\text{faradaic}}\left(R_{ct,1} + \frac{R_{\text{part}}}{Y_s}\right) = (\tilde{\Phi}_1 - \tilde{\Phi}_{1f}) \quad [21]$$

The impedance for the faradaic reaction is defined as the ratio of the potential across the interface to the faradaic current density

$$Z_{\text{faradaic}} = R_{ct,1} + \frac{R_{\text{part}}}{Y_s} = R_{ct,1} + R_{\text{part}}\frac{\tanh\left(\sqrt{j\Omega_s}\right)}{\sqrt{j\Omega_s} - \tanh\sqrt{j\Omega_s}} \quad [22]$$

This expression can be resolved into real and imaginary components with the identities

$$\sqrt{j} = \frac{j+1}{2} \quad [23]$$

and, from Abramowitz and Stegun[10]

$$\tanh(x + jy) = \frac{\sinh 2x + j\sin 2y}{\cosh 2x + \cos 2y} \quad [24]$$

but the resulting expressions are not particularly enlightening, and care must be taken in evaluating them. The real and imaginary components can be tricky to evaluate numerically due to the differences between very small or very large quantities in the expansions. Rather than focusing on these large expressions and the details of calculating them numerically, we evaluate some limiting cases which are appropriate to use in various frequency ranges.

Limiting cases: moderately high frequencies.—We can also examine the limiting cases. In the limit as $\Omega_s >> 1$, $\tanh(\sqrt{j\Omega_s}) \to 1$.[10] If one considers moderately high frequencies, at which $\tanh(\sqrt{j\Omega_s}) \approx 1$ but Ω_s is not much greater than unity, one obtains the following result

$$Y_s \approx \sqrt{j\Omega_s} - 1$$
$$Z_{\text{faradaic}} \approx R_{ct,1} + \frac{R_{\text{part}}}{\sqrt{2\Omega_s}}\left[\frac{(1-j) - \sqrt{\frac{2}{\Omega_s}}}{1 - \sqrt{\frac{2}{\Omega_s}} + \frac{1}{\Omega_s}}\right] \quad [25]$$

The admittance in this frequency range can be written as

$$Y_{\text{faradaic}} \approx \frac{1}{R_{ct,1}} - \frac{R_{\text{part}}}{R_{ct,1}^2}\frac{1}{\sqrt{2\Omega_s}}\left[\frac{(1-j) - (1 - R_{\text{part}}/R_{ct,1})\sqrt{\frac{2}{\Omega_s}}}{(1 - R_{\text{part}}/R_{ct,1})\sqrt{\frac{2}{\Omega_s}} + (1 - R_{\text{part}}/R_{ct,1})^2\frac{1}{\Omega_s}}\right] \quad [26]$$

Equations 25 and 26 give the result for the diffusion impedance when the frequency is small enough that the curvature of the particle affects the penetration depth, but not so small that this penetration depth reaches the center of the particle.

Limiting cases: high frequencies.—If Ω_s is large enough, it is possible to neglect entirely the hyperbolic tangent term and retain only the highest-order terms in Ω_s. This yields the limit of the semi-infinite Warburg impedance, as was derived for a planar film by Ho *et al.*[1] In this limit, the diffusion length scale is much less than the dimension of the particle

$$Z_{\text{faradaic}} \approx R_{ct,1} + \frac{R_{\text{part}}}{\sqrt{2\Omega_s}}(1-j) = R_{ct,1} + \left(-\frac{\partial U}{\partial c_s}\right)\frac{1}{F}(2\omega D_s)^{-1/2}(1-j) \quad [27]$$

$$Y_{\text{faradaic}} \approx \frac{1}{R_{ct,1}} - \frac{R_{\text{part}}}{R_{ct,1}^2}\frac{(1-j)}{\sqrt{2\Omega_s}} = \frac{1}{R_{ct,1}} + \left(-\frac{\partial U}{\partial c_s}\right)\frac{1}{FR_{ct,1}^2}(2\omega D_s)^{-1/2}(j-1)$$

Limiting case: low frequencies.—We can also examine the limit as $\Omega_s \to 0$. These are cases where the time constant is sufficiently large that diffusion processes can access the entire depth of the particle. These results are similar to those found in the work of Armstrong[11] and Jacobsen and West.[12] The Taylor series expansion for $\tanh y$ is[10]

$$\tanh y = y - \frac{1}{3}y^3 + \frac{2}{15}y^5 + \cdots \quad [28]$$

After an expansion of Z_{faradaic}, we find

$$Z_{\text{faradaic}} = R_{ct,1} + \frac{1}{5}R_{\text{part}} - j\frac{3R_{\text{part}}}{\Omega_s} \quad [29]$$

Alternatively, this can be written as

$$Z_{\text{faradaic}} = \left(R_{ct,1} + \frac{1}{5}R_{\text{part}}\right) - \frac{j}{\omega C_{\text{part}}} \quad [30]$$

where

$$C_{\text{part}} = \frac{R_s}{3}\frac{F}{\left(-\frac{\partial U}{\partial c_s}\right)} \quad [31]$$

Or as an admittance

S0013-4651(99)12-086-X CCC: $7.00 © The Electrochemical Society, Inc.

$$Y_{\text{faradaic}} = (5R_{\text{ct},1} + R_{\text{part}})\frac{1}{5}\left(\frac{\Omega_s}{3R_{\text{part}}}\right)^2 + j\frac{\Omega_s}{3R_{\text{part}}}$$

$$= \left(R_{\text{ct},1} + \frac{1}{5}R_{\text{part}}\right)(\omega C_{\text{part}})^2 + j\omega C_{\text{part}} \quad [32]$$

This low-frequency limit corresponds to the case when the frequency is so low that the particle behaves like a capacitor. The passage of current draws material from the particle, and, in this low-frequency range, the change in concentration corresponds to a depletion of the total amount of intercalant inside the particle rather than to a concentration profile which penetrates only partway into the particle. It is not the complete depletion of the particle, but rather the emptying of the particle to the extent possible given the change in OCP with particle concentration. We see that C_{part}, the capacity per unit area, is the product of the ratio of particle volume to area ($R_s/3$), multiplied by the capacity of the solid material per unit volume of solid material. It is worthwhile to note that the capacitive response, governed by C_{part}, exists even when the solid-phase diffusion coefficient is infinite, because while R_{part} is inversely proportional to D_s, the capacity of the particle, corresponding to the amount of active material stored within it, is independent of D_s.

Overall single-particle impedance.—The results of the previous section describe the impedance of the faradaic reaction at the film/solution interface. The structure of the particle and film shown schematically in Fig. 1 indicates that there are additional paths through which current might flow and additional resistances which impede the passage of current. These additional impedances and admittances must be considered to describe the overall particle impedance.

First we consider the charging of the double layer at the particle/film interface

$$\tilde{i}_{\text{dl},1} = j\omega C_{\text{dl},1}(\tilde{\Phi}_1 - \tilde{\Phi}_{1f}) \quad [33]$$

Writing the total interfacial current density as the sum of the faradaic and double-layer-charging current densities, we find

$$\tilde{i}_n = \left[\frac{1}{R_{\text{ct},1} + \dfrac{R_{\text{part}}}{Y_S}} + j\omega C_{\text{dl},1}\right](\tilde{\Phi}_1 - \tilde{\Phi}_{1f}) \quad [34]$$

Neglecting the variation of OCP on the concentration of intercalant in the film or in solution, we write the relation between current density across the interface and the potential difference at the outer interface

$$\tilde{i}_n = \left[\frac{1}{R_{\text{ct},2}} + j\omega C_{\text{dl},2}\right](\tilde{\Phi}_{2f} - \tilde{\Phi}_2) \quad [35]$$

Incorporating the ohmic resistance of the film from Eq. 7, we can sum these impedances to find the transfer function between current density through the film and the potential difference between the solid particle and the adjacent solution

$$\tilde{i}_n\left[\frac{R_{\text{ct},1} + \dfrac{R_{\text{part}}}{Y_s}}{1 + j\omega C_{\text{dl},1}\left(R_{\text{ct},1} + \dfrac{R_{\text{part}}}{Y_s}\right)} + R_{\text{film}} + \frac{R_{\text{ct},2}}{1 + j\omega R_{\text{ct},2}C_{\text{dl},1}}\right] = (\tilde{\Phi}_1 - \tilde{\Phi}_2) \quad [36]$$

Finally, we can add this current density to the current density which flows as a result of charging the film capacitance (from Eq. 8) to relate the total current per unit interfacial area to the potential difference between the solid and solution

$$\tilde{I}_n = \left(\frac{1}{\left[\dfrac{R_{\text{ct},1} + \dfrac{R_{\text{part}}}{Y_s}}{1 + j\omega C_{\text{dl},1}\left[R_{\text{ct},1} + \dfrac{R_{\text{part}}}{Y_s}\right]} + R_{\text{film}} + \dfrac{R_{\text{ct},2}}{1 + j\omega R_{\text{ct},2}C_{\text{dl},2}}\right]} + j\omega C_{\text{film}}\right)(\tilde{\Phi}_1 - \tilde{\Phi}_2) \quad [37]$$

We can express this transfer function either as an admittance, $Y = \tilde{I}_n/(\tilde{\Phi}_1 - \tilde{\Phi}_2)$, or as an impedance, $Z = (\tilde{\Phi}_1 - \tilde{\Phi}_2)/\tilde{I}_n$.

Characteristic time constants.—In the examination of the case of a single intercalation particle without an insulating film, there are several discernable time constants which are relevant to the processes which occur in the particle. The first of these is the resistive-capacitance (RC) time constant which characterizes the frequency range over which the current at the interface is shifted from purely capacitive to purely resistive

$$\omega_{\text{RC}} = (R_{\text{ct},1}C_{\text{dl},1})^{-1} \quad [38]$$

The time constant which is relevant to solid-phase diffusion over the length scale of the particle radius is given by the ratio of the solid-phase diffusion coefficient to the square of the particle radius

$$\omega_{\text{part}} = \frac{D_s}{R_s^2} \quad [39]$$

In the high-frequency limit of solid-phase diffusion, Eq. 27 shows that there is not a characteristic time constant for this result; the impedance is proportional to a constant multiplied by $\omega^{-1/2}$, and there is no maximum in the impedance corresponding to a particular frequency. If, however, one wishes to consider the frequency at which the solid-phase diffusion in this high-frequency limit is comparable to the charge-transfer resistance, one can determine the frequency below which the ratio of $R_{\text{part}}/\sqrt{2\Omega_s}$ to $R_{\text{ct},1}$ is greater than 5%, which yields a time constant

$$\omega_D = 0.05^{-2}\left(-\frac{\partial U}{\partial c_s}\right)^2\left(\frac{1}{R_{\text{ct},1}F}\right)^2\frac{1}{2D_s}$$

$$= \left[20\left(-\frac{\partial U}{\partial c_s}\right)\frac{i_{0,1}(\alpha_a + \alpha_c}{RT}\right]^2\frac{1}{2D_s} \quad [40]$$

Finally, one can calculate a time constant for the low-frequency capacitive limit of the particle. This does not constitute a transition frequency, as the resistance and capacitance are in series, while the charge-transfer resistance and double-layer capacitance are in parallel, but at $\omega = \omega_{\text{RC}_{\text{part}}}$, where

$$\omega_{\text{RC}_{\text{part}}} = \left[\left(R_{\text{ct},1} + \frac{1}{5}R_{\text{part}}\right)C_{\text{part}}\right]^{-1} \quad [41]$$

the imaginary component of the capacitive limit has the same magnitude as the real component of that limit. These time constants are tabulated and included with the physical properties in Tables I-III.

S0013-4651(99)12-086-X CCC: $7.00

Table I. Electrode parameters for use in single-particle simulations, with insulating film and charge-transfer resistance at film-solution interface. This is the most complicated interface and includes nonzero values for all the parameters necessary to describe the full particle shown in Fig. 1.

Property	Value
$C_{dl,1}$	10 μF/cm^2
$i_{0,1}$	0.69 mA/cm^2
$\alpha_a + \alpha_c$	1
T	353.15 K
$R_{ct,1}$	44.06 Ω cm^2
$-\left(\frac{\partial U}{\partial c_s}\right)$	20.27 V cm^3/mol
D_s	1.0×10^{-9} cm^2/s
R_s	2.0 μm
R_{part}	42.021 Ω cm^2
R_{film}	1100 Ω cm^2
C_{film}	10 pF/cm^2
$R_{ct,2}$	4.4 Ω cm^2
$C_{dl,2}$	10 μF/cm^2
ω_{RC}	361 Hz
ω_D	0.724 Hz
ω_{part}	3.98 mHz
ω_{RCpart}	9.56 mHz

Table II. Parameters for use in single-particle simulations, with an insulating film but without an external interfacial impedance and without electrochemical double-layer capacitance.

Property	Value
$C_{dl,1}$	0
$i_{0,1}$	28.2 mA/cm^2
$\alpha_a + \alpha_c$	1
T	298 K
$R_{ct,1}$	0.91 Ω cm^2
$-\left(\frac{\partial U}{\partial c_s}\right)$	27.69 V cm^3/mol
D_s	3.9×10^{-10} cm^2/s
R_s	12.5 μm
R_{part}	919.8 Ω cm^2
R_{film}	1100 Ω cm^2
C_{film}	20 μF/cm^2
$R_{ct,2}$	0
$C_{dl,2}$	0
ω_{RC}	—
ω_D	8.12 Hz
ω_{part}	3.97×10^{-5} Hz
ω_{RCpart}	3.74 mHz

Table III. Parameters for use in single-particle electrode simulations. This is the simplest form of the particle under consideration. There is no insulating film and, consequently, only the faradaic and double-layer charging processes contribute to the overall impedance.

Property	Value
$C_{dl,1}$	10 μF/cm^2
$i_{0,1}$	0.69 mA/cm^2
$\alpha_a + \alpha_c$	1
T	353.15 K
$R_{ct,1}$	44.06 Ω cm^2
$-\left(\frac{\partial U}{\partial c_s}\right)$	20.27 V cm^3/mol
D_s	1.0×10^{-9} cm^2/s
R_s	2.0 μm
R_{part}	42.021 Ω cm^2
R_{film}	0
C_{film}	0
$R_{ct,2}$	0
$C_{dl,2}$	0
ω_{RC}	361 Hz
ω_D	0.724 Hz
ω_{part}	3.98 mHz
ω_{RCpart}	9.56 mHz

Porous Electrodes

Particle-size distribution.—Once we have determined the impedance response of a single particle, we can combine this transfer function with a description of the porous electrode. We can write a balance on the fractrion of total current flowing in solution to find that

$$\frac{\partial \tilde{i}_2}{\partial x} = \sum_j N(r_j) 4\pi r_j^2 \tilde{I}_n(r_j) \qquad [42]$$

where $N(r_j)$ is the number of particles per unit volume of electrode with a radius r_j, $4\pi r_j^2$ is the surface area per particle, and $\tilde{I}_n(r_j)$ is the normal current per unit surface area of a particle of that size. The general form of $\tilde{I}_n$ is a function of the potential difference between the solid and solution, as given by Eq. 37. Defining $Y(r_j)$ as the transfer function which relates the outward normal current density per unit surface area of a particle to the potential difference, we write

$$\frac{\partial \tilde{i}_2}{\partial x} = \left(\sum_j N(r_j) 4\pi r_j^2 Y(r_j)\right)(\tilde{\Phi}_1 - \tilde{\Phi}_2) \qquad [43]$$

A schematic diagram which represents the structure of the porous electrode is shown in Fig. 2. The flow of current from one phase to another is shown schematically in Fig. 3. The flow of current across the interface of the particle allows the current to move from the solution phase to the solid phase as one traverses the length of the porous electrode.

This can be generalized to consider a continuous particle-size distribution function. With $N(r)dr$ being the number of particles per unit volume of composite electrode with a radius between size r and $r + dr$, we can write that

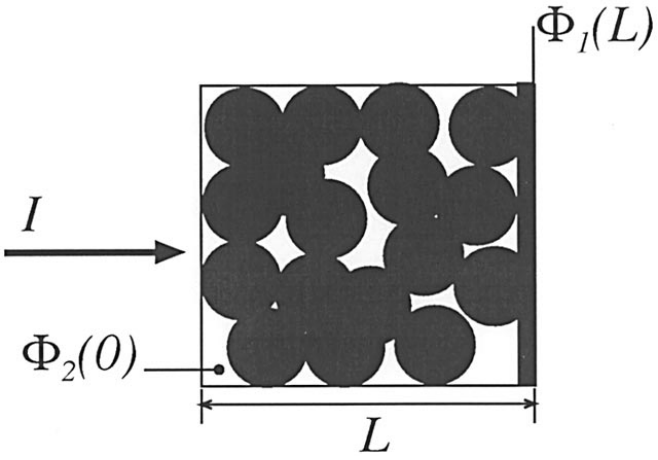

Figure 2. Schematic diagram showing the construction of a porous electrode consisting of spherical particles.

S0013-4651(99)12-086-X CCC: $7.00

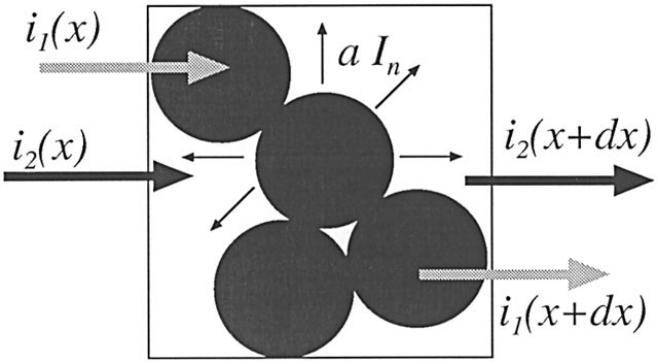

Figure 3. Schematic diagram showing the differential flow of current in a porous electrode in which current can flow in both the solid and solution phases.

$$a = 4\pi\int_0^\infty N(r)r^2dr$$
$$\epsilon_s = \frac{4}{3}\pi\int_0^\infty N(r)r^3dr \qquad [44]$$

where a is the interfacial surface area of the particles per unit volume of electrode and ϵ_s is the volume fraction of solid in the composite electrode. Then

$$\frac{\partial\tilde{i}_2}{\partial x} = \left(4\pi\int_0^\infty N(r)Y(r)r^2dr\right)(\tilde{\Phi}_1 - \tilde{\Phi}_2) = \overline{aY}(\tilde{\Phi}_1 - \tilde{\Phi}_2) \qquad [45]$$

The quantity $\overline{aY}$ is the interfacial admittance per unit volume of electrode, averaged over the particle-size distribution. Equation 45 relates the divergence of the solution-phase current to the local potential difference between solid phase and solution phase.

For this work, we propose a distribution of the form

$$N(r)dr = \left[\frac{a^3 e^{-\left(\frac{\psi}{4}\right)^2}}{(4\pi)9\epsilon_s^2\sqrt{\pi}\psi}\right]\exp\left[-\left(\frac{\ln\left(\frac{ra}{3\epsilon_s}\right)}{\psi}\right)^2\right]\exp\left[-\frac{5}{2}\ln\left(\frac{ra}{3\epsilon_s}\right)\right]\frac{dr}{r} \qquad [46]$$

where ψ is a parameter which determines the sharpness of the distribution. This function is a Gaussian distribution in the logarithm of the particle size. Defining the distribution in this way allows one to select values of the specific surface area a and the volume fraction of solid material ϵ_s and vary only the breadth of the distribution.

It can be shown that $\psi = \sqrt{(\ln(\bar{r}a/3\epsilon_s)}$, where $\bar{r}$ is the mean particle radius, averaged over the particle size distribution

$$\bar{r} = \frac{\int_0^\infty N(r)rdr}{\int_0^\infty N(r)dr} \qquad [47]$$

The values of a and ϵ_s can be determined from experiment, and one can then explore the affect of various particle-size distributions which yield the determined values of a and ϵ_s. Graphs of the area distribution and volume distribution for several values of the parameter ψ are shown in Fig. 4. As ψ approaches zero, the distribution functions approach the limit of a delta function.

Impedance of porous electrodes.—In the porous electrode, we consider total current, $\tilde{I}$, to equal the current carried in the solution phase, $\tilde{i}_2$, plus the current carried in the solid conducting phase. Ohm's law is obeyed in each phase. In this paper, we neglect the concentration variations in the solution phase which result from small diffusion coefficients or nonunity transference numbers

$$\frac{\partial\tilde{\Phi}_1}{\partial x} = -\frac{\tilde{I} - \tilde{i}_2}{\sigma}$$
$$\frac{\partial\tilde{\Phi}_2}{\partial x} = -\frac{\tilde{i}_2}{\kappa} \qquad [48]$$
$$\frac{\partial}{\partial x}(\tilde{\Phi}_1 - \tilde{\Phi}_2) = -\frac{\tilde{I}}{\sigma} + \left(\frac{1}{\sigma} + \frac{1}{\kappa}\right)\tilde{i}_2$$

Combining this expression with our current balance (Eq. 45) and making the position variable dimensionless with the thickness of the porous electrode L, we find

$$\frac{d^2}{d\zeta^2}(\tilde{\Phi}_1 - \tilde{\Phi}_2) = \left(\frac{L}{\sigma} + \frac{L}{\kappa}\right)\left(\overline{aY}L\right)(\tilde{\Phi}_1 - \tilde{\Phi}_2) \qquad [49]$$

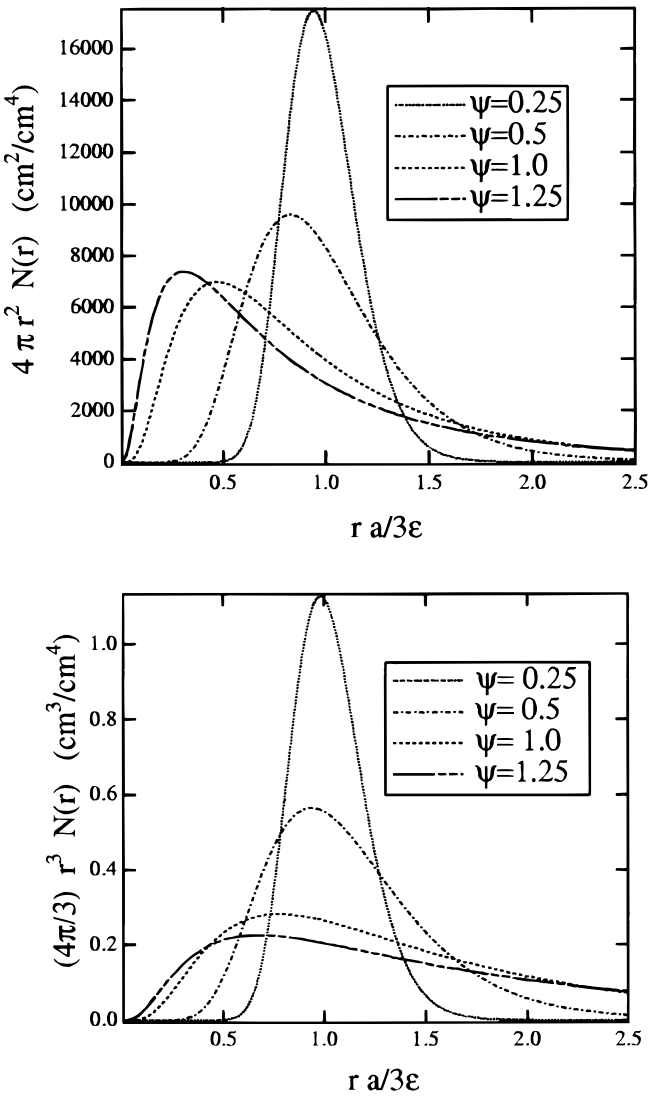

Figure 4. Diagram showing contribution to total specific surface area and total volume of particles for various values of ψ in $N(r)dr$. The function becomes a delta function as $\psi \to 0$.

S0013-4651(99)12-086-X CCC: $7.00

where $\overline{aY}$ is the average admittance of all particles in the composite electrode, as given in Eq. 45. This differential equation is solved subject to the boundary conditions

$$\begin{aligned} \tilde{i}_2 &= \tilde{I} \quad \text{at } \zeta = 0 \\ \tilde{i}_2 &= 0 \quad \text{at } \zeta = 1 \end{aligned} \qquad [50]$$

that is, all the current is carried in solution at the separator/porous electrode interface, and all the current is in the solid phase at the current collector. This has the solution

$$Z = \frac{\tilde{\Phi}_1(L) - \tilde{\Phi}_2(0)}{I} = \frac{L}{\kappa + \sigma}\left[1 + \frac{2 + \left(\frac{\sigma}{\kappa} + \frac{\kappa}{\sigma}\right)\cosh\nu}{\nu \sinh\nu}\right] \qquad [51]$$

where

$$\frac{L}{\nu} = \left(\frac{\kappa\sigma}{\kappa + \sigma}\right)^{1/2}\left(\overline{aY}\right)^{-1/2} \qquad [52]$$

Equations 51 and 52 are satisfying because they reveal the extension of the solution for linear kinetics set forth by Newman.[13] In the example provided in Ref. 13, aY is simply represented by $a\, i_0 F(\alpha_a + \alpha_c)/RT$, the faradaic impedance for simple linear kinetics.

The result shown here is more general and allows one to specify a general form for the particle admittance and particle-size distribution. If the admittance of the particle is dictated only by charge transfer, Eq. 52 reduces to the form set forth in Ref. 13. See also Ong and Newman[14] for a similar result for the transient response of a porous electrode with double-layer capacitance included.

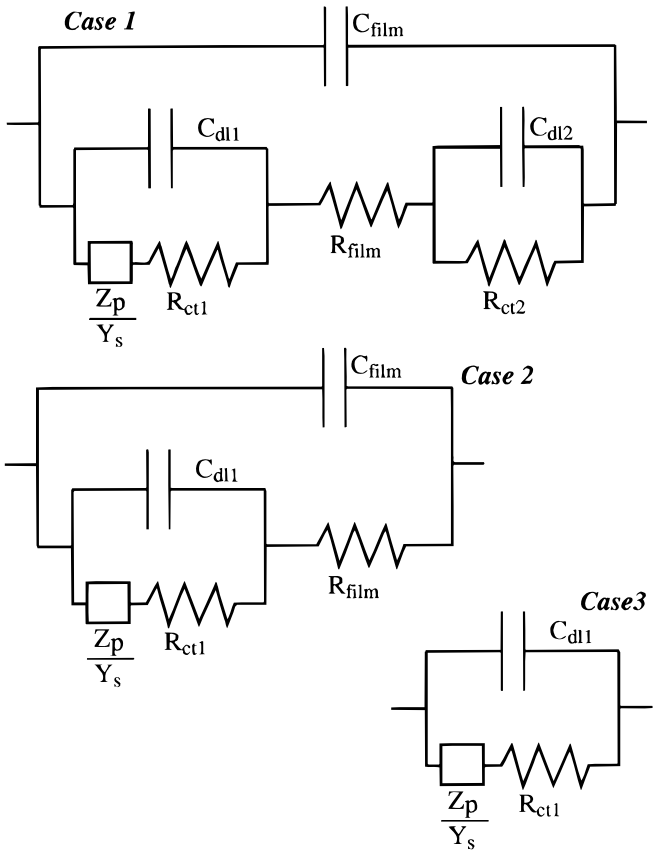

Figure 5. Schematic diagram of the cases considered for simulations of single intercalation particles. Case 1 is the most general case, shown schematically in Fig. 1, and it includes both internal and external interfacial impedances, as well as a resistive film. Case 2 neglects the external interfacial impedance and the internal double layer. Case 3, the simplest case which is considered, neglects the insulating film entirely. Values for the parameters are shown in Tables I-III.

Table IV. Electrode parameters for use in porous electrode simulations. Other parameters are the same as in Table III unless otherwise noted.

Property	Value
ϵ_s	0.5
a	7500 cm^{-1}
L_+	100 μm
κ	55 μS/cm
σ	1.0 S/cm

Results and Discussion

We solve the equations to determine the impedance response first of a single particle and then of a porous electrode composed of these particles. For the impedance response of single particles, we consider first the full case shown in Fig. 1 (case 1 in Fig. 5). After noting the general features of the impedance spectra, we attempt to examine the system in greater depth by next considering a system without an external interfacial impedance (case 2 in Fig. 5). Finally, we consider a particle without an insulating film (case 3 in Fig. 5). This simplest case is the particle which shall be incorporated into the porous electrode model to examine the effect of a reaction rate which becomes distributed throughout the depth of the electrode by a balance of the particle impedance with the ohmic drop. The physical properties of the particles are shown in Tables I-III. The relevant properties of the porous electrode are listed in Table IV.

First, we consider the most general description of the impedance spectrum of a single particle: a particle with an insulating film and an external interfacial impedance as well. The results are shown in Fig. 6 and 7. Figure 6 shows the impedance of a single particle plotted in a complex-plane graph; Fig. 7 shows the results of magnitude and phase angle plotted *vs.* frequency of the applied signal. We have adopted the notation that Z' is the real portion of the complex impedance; Z'' is the imaginary portion.

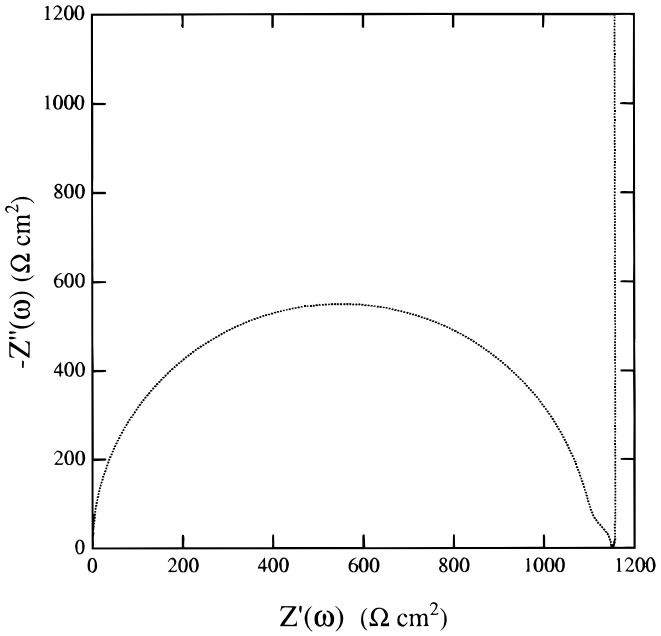

Figure 6. Complex-plane plot of impedance of a single particle for case 1: interfacial impedance with insulating film and solid-phase diffusion and outer interfacial impedance.

S0013-4651(99)12-086-X CCC: $7.00

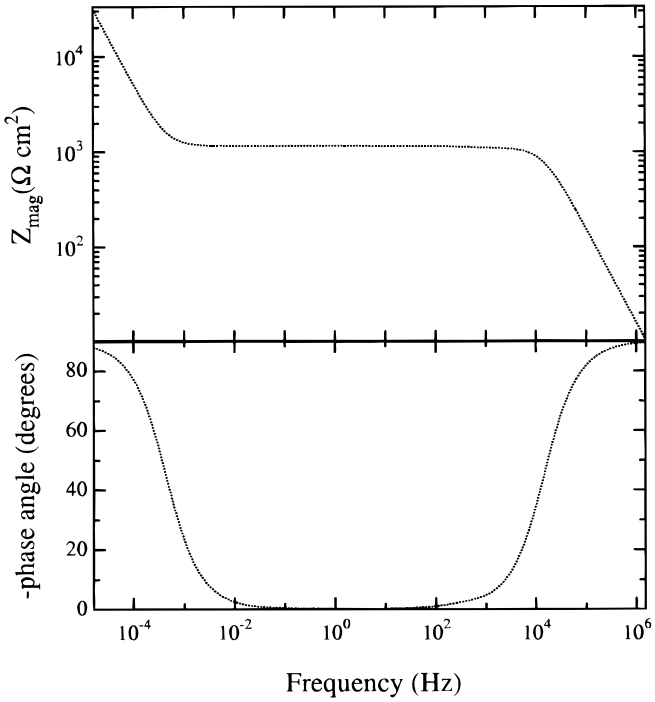

Figure 7. Phase angle and magnitude of complex single-particle impedance for case 1: interfacial impedance with insulating film and solid-phase diffusion and outer interfacial impedance.

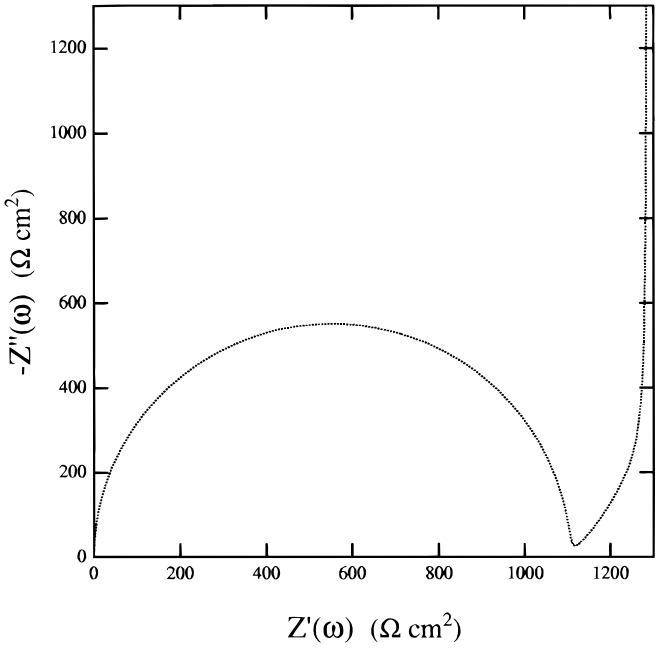

Figure 8. Complex-plane plot of impedance of a single particle for case 2: interfacial impedance with insulating film and solid-phase diffusion; no outer interfacial impedance or inner double layer.

There is overlap of the time constants of the charging of the two double layers, and at sufficiently high frequencies the capacitance of the film shorts the film resistance. There is sufficient difference between the time constants for diffusion and for double-layer charging that the impedance lies on the real-axis for a significant range of intermediate frequencies. For frequencies between approximately 100 mHz and 100 Hz, the impedance response varies little; none of the processes has time constants in this frequency range.

It is difficult to distinguish among the double-layer and film capacitances in this case; many of the processes occur with similar time constants such that the impedance spectra resemble a resistor and capacitor in parallel (the film's resistive and capacitive characteristics), both of which are in series with the capacitance of the particle. There is a shoulder on the low-frequency end of the RC loop, but relevant information cannot be gleaned from this detail.

Let us consider next a simpler system by examining a particle with a film but without an internal double layer and without external interfacial impedance. The values shown in Table II are typical values used in lithium-battery simulations for carbon electrodes.[14,15] Here we have charge-transfer and film resistance, along with solid-phase diffusion resistance, which is shorted at higher frequencies by the capacitance of the film. Data for these simulations are given in Fig. 8 and 9. Here the time constant for the film capacitance in parallel with the faradaic impedance is not completely separated from that for particle diffusion; the impedance does not return all the way to the real-axis at intermediate frequencies. Some of the general features of single-particle impedance are more clear in this example. There is the parallel-RC loop at high frequencies, and the impedance is dominated by diffusive elements and, eventually, the capacity of the particle capacitance at much lower frequencies.

In order to study these effects further, we simplify the system even further by examining a particle without an insulating film. Figure 10 includes plots of the impedance of the particle using the values of the parameters shown in Table III and also results for two other values of D_s. The effect of D_s on the impedance is discussed below. Figure 11 shows clearly the capacitive behavior of the particle. The interfacial current is purely capacitive at high frequencies; lack of a solution-phase ohmic or diffusional impedance in series with the interface forces the phase angle back to 90° in the high-frequency limit as the current becomes purely capacitive. One can be a slope of -1 at sufficiently low frequencies in the magnitude *vs.* frequency plot of Fig. 11, but there is not sufficient resolution of the time constants to resolve a separate slope of $-1/2$ for diffusive control for the case where $D_s = 1 \times 10^{-9}$ cm^2/s.

The standard RC semicircle is evident at high frequencies, where the charge-transfer resistance and double-layer capacitance are in parallel. At lower frequencies, the double layer becomes blocking,

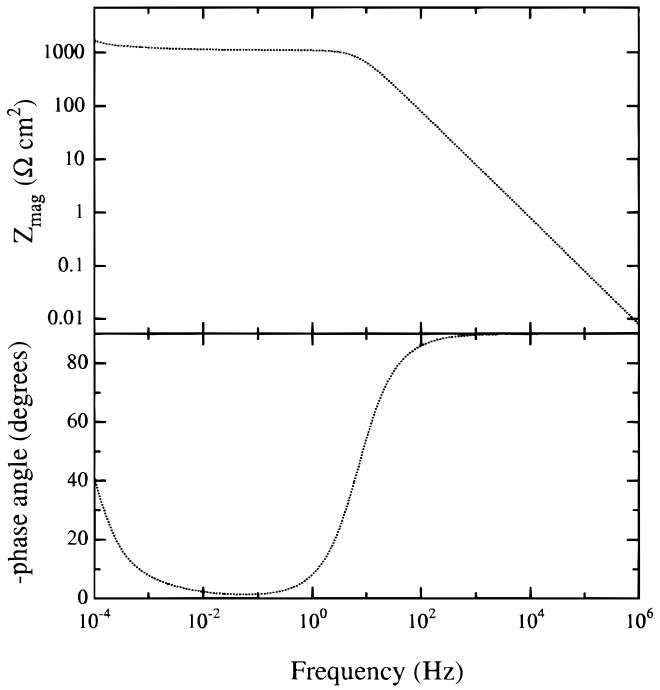

Figure 9. Phase angle and magnitude of complex single-particle impedance for case 2: interfacial impedance with insulating film and solid-phase diffusion; no outer interfacial impedance or inner double layer.

S0013-4651(99)12-086-X CCC: $7.00

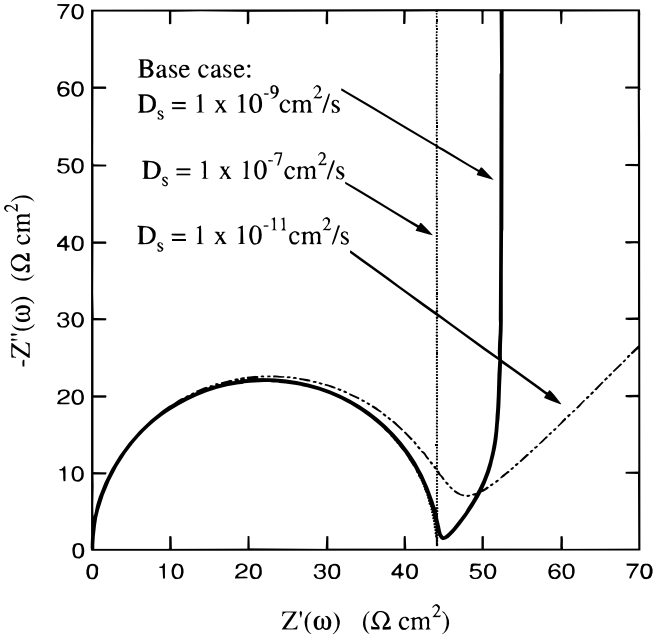

Figure 10. Complex-plane plot of impedance of a single particle for case 3: interfacial impedance with solid-phase diffusion limitations but no insulating film. Also shown in the figure are results for two different values of the solid-phase diffusion coefficient D_s.

and all the current flows through the faradaic path. As the frequency is decreased even more, the solid-phase diffusion impedance becomes the most pronounced feature, and at even lower frequencies, the capacity of the solid particle dominates. Although the time consants for the double-layer and solid-phase diffusion differ by approximately three orders of magnitude (cf. Table III), the two processes are not completely resolved in the sense that the impedance does not return all the way to the real-axis as we decrease the frequency from ω_{RC} before the imaginary component increases in magnitude as diffusive processes become more important. The different contributions to the overall impedance also depend upon the frequency in different ways (the RC loop decreases roughly linearly with ω on the low-frequency side of the loop and the diffusion impedance increases with $\omega^{-1/2}$), and there can still be overlap despite the separation of the time constants.

It is important to note that in the cases considered here, the frequency which is characteristic of diffusion in the particle (ω_{part}) is smaller than the frequency which is characteristic of the capacity of the particle ($\omega_{RC_{part}}$). The results of Eq. 30 and 32 are limiting cases for the low-frequency limit, but diffusive effects are still important at the frequency where the imaginary component of the low-frequency limit is the same size as the real component. When the frequency is equal to $\omega_{RC_{part}}$, then the impedance is not given by the limiting form expressed by Eq. 30. This capacitive limit is reached eventually but at frequencies still lower than ω_D.

Figure 10 also shows the effect of changing the solid-phase diffusion coefficient on the impedance of a single intercalant particle. The figure reveals that for the base case, for a diffusion coefficient of 1×10^{-9} cm^2/s, there is overlap of the interfacial process and solid-phase diffusion. The double layer is still not completely blocking at frequencies low enough that the solid-phase diffusion process contributes significantly to the impedance of the particle.

If the solid-phase diffusion coefficient is decreased by two orders of magnitude to 1×10^{-11} cm^2/s, the frequency below which the solid phase becomes controlling is also decreased by a factor of 100, but this change increases the magnitude of the solid-phase diffusion impedance according to Eq. 27. Even though the time constant is shifted to imply a greater resolution of frequencies, the magnitude of the solid-phase-diffusion impedance is increased so that it interferes with the charge transfer and double-layer impedance even when ω is much greater than ω_{part}. When the diffusion coefficient is increased to 1×10^{-7} cm^2/s, the diffusive component of the particle impedance is lowered, and the response approaches the limit of purely capacitive behavior in the solid particle.

Figure 12 displays the effect of changing the slope of the OCP of the particle with respect to intercalant concentration. Changing this parameter does not change the relevant time constant for diffusion in the particle, but it does change the magnitude of the solid-phase im-

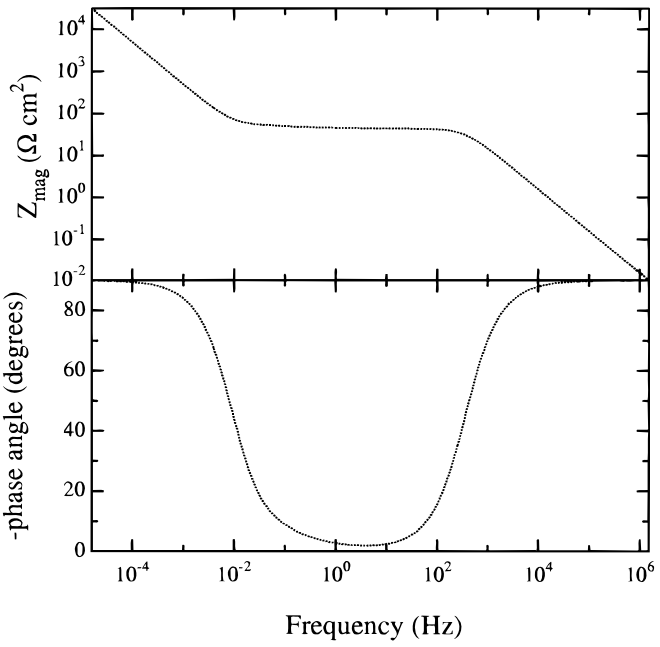

Figure 11. Phase angle and magnitude of complex single-particle impedance for case 3: interfacial impedance with solid-phase diffusion limitations but no insulating film.

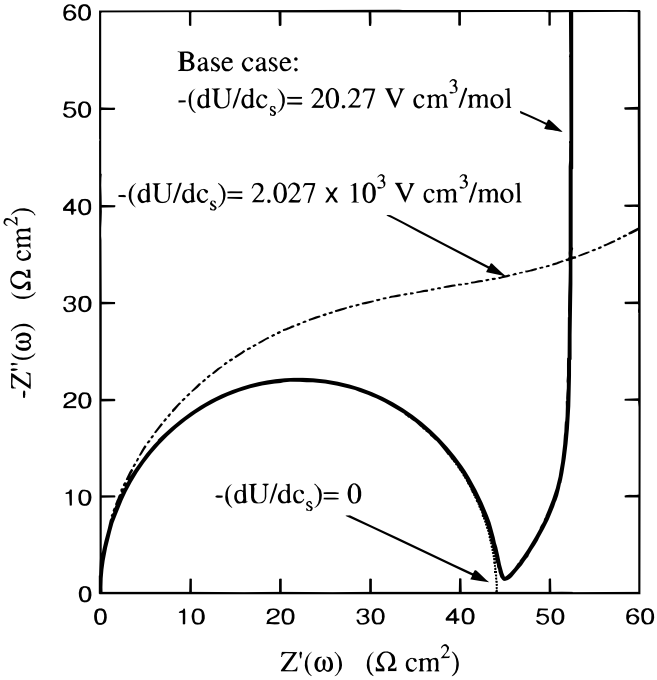

Figure 12. Complex-plane plot of impedance of single particle: effect of slope of OCP. (—) The slope of OCP which corresponds to the value in Table III.

S0013-4651(99)12-086-X CCC: $7.00

pedance, as indicated by Eq. 20, and therefore shifts the frequency at which the diffusion impedance in the solid is comparable in magnitude to the charge-transfer resistance. We note that there is no solid-phase impedance in the case where the slope of the OCP is zero. All the impedance of the particle, in this case, is determined by the charge-transfer resistance and the capacitance of the double layer.

Limiting cases: diffusion control.—For the base case without an insulating film, examination of the asymptotes describes previously shows that for both the real and imaginary components of the diffusion impedance, the high-frequency limit of the solid-phase-diffusion impedance varies as $\omega^{-1/2}$. The simulation result and this asymptote are plotted in the upper graph of Fig. 13, but we note that the double-layer capacitance at high frequencies and the other terms in Eq. 25 obscure the diffusion impedance at small values of $\omega^{-1/2}$ (large values of ω) due to the overlap of time constants.

The slopes of the real and imaginary components of the impedance are independent of particle size. This result should provide a way to determine the solid-phase diffusion coefficient D_s even if the particle size is not known. The interference of the interfacial impedance, however, restricts the range of applicability of this asymptote and can make it difficult to determine diffusion coefficients in this manner. The difficulty of measuring diffusion coefficients with impedance data is discussed further in a paper by Doyle *et al.*[16]

Limiting cases: low-frequency limit.—We also examine the low-frequency limit where solid-phase capacity dominates the impedance in the lower graph in Fig. 13. This result does yield the purely capacitive response at very low frequencies, but the imaginary component of the impedance in this limit provides no information about the solid-phase diffusion coefficient (cf. Eq. 30). This limit is obtained only at very low frequencies, in the millihertz range for the simple case, for example. These frequencies are probably not, in general, experimentally accessible, because the filling of the intercalation particle (the process under consideration) can be obscured by side reactions and other processes occurring in the cell with similar time constants.

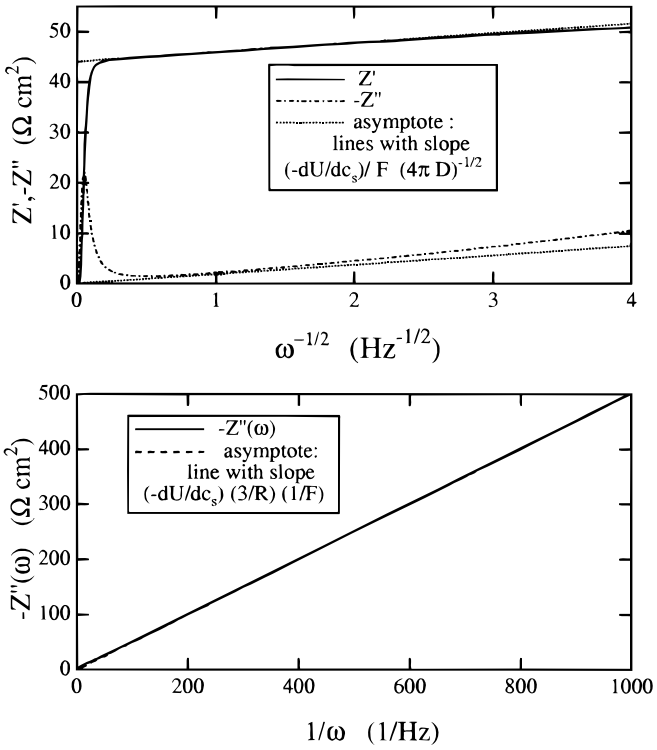

Figure 13. Asymptotic limits of solid-phase diffusion impedance. Results shown are for case 1: no insulating film and no outer interface.

Effect of porous electrodes.—We have examined the behavior of a single particle, and examined the limiting forms of the impedance response for a particle without an insulating film. The impedance response of a single particle can then be incorporated into Eq. 51 to determine the impedance of a porous electrode composed of a continuum of these particles for a variety of particle-size distributions. The results of these simulations are shown as complex-plane plots in Fig. 14 and as plots of magnitude and phase angle *vs.* frequency in Fig. 15. Since the specific surface area *a* is prescribed and the charge-transfer and double-layer impedance depend only upon the surface area of the particle, the impedance at high frequencies is independent of the particle-size distribution. At lower frequencies, when the solid-phase diffusion limitations become important, we see that the particle-size distribution becomes very important. Figure 14 shows a complex-plane plot of the porous electrode impedance on two different scales for the impedance properties indicated by Table III and the electrode properties shown in Table IV.

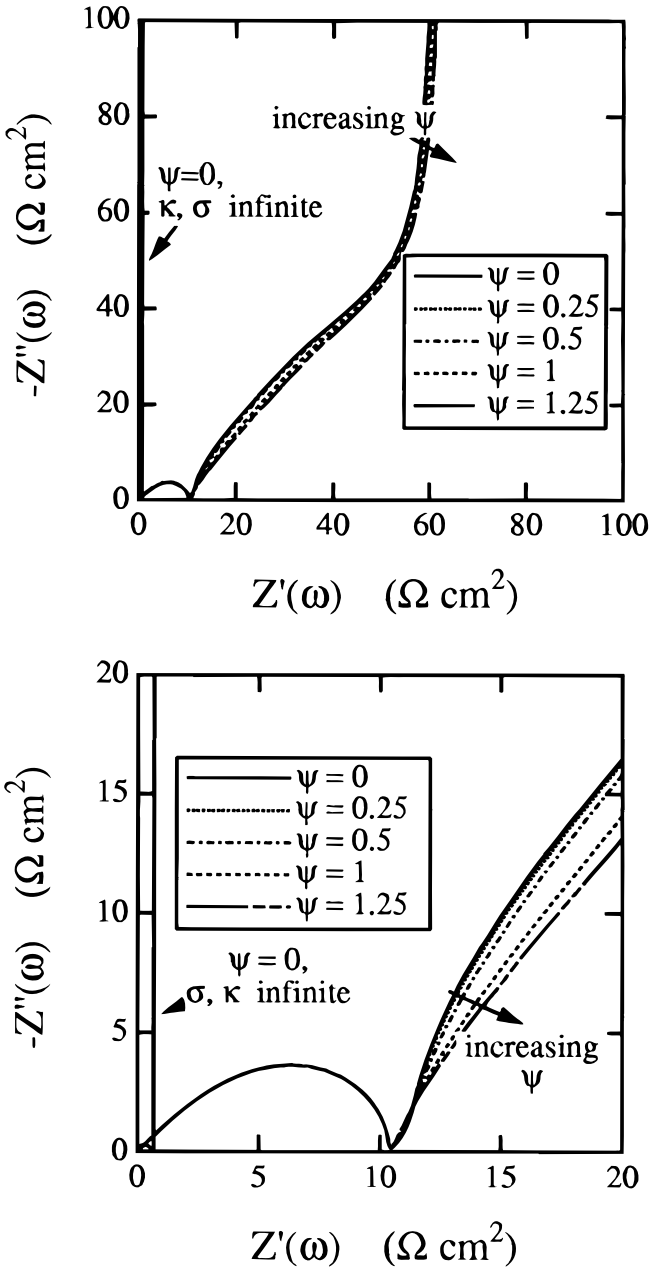

Figure 14. Complex-plane plots of the impedance of a porous electrode for various particle-size distributions. The lower figure is an expanded view.

S0013-4651(99)12-086-X CCC: $7.00

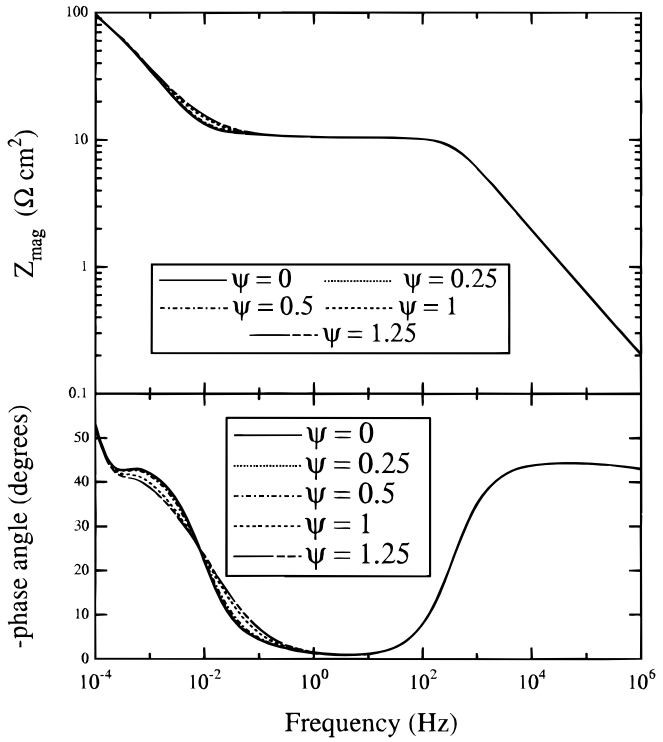

Figure 15. Bode plots of impedance of porous electrode for various particle-size distributions.

At the high-frequency limit, there is clearly a 45° asymptote originating from the real-axis. This is not due to diffusional effects (the Warburg impedance yields a 45° in the high-frequency limit as well). Rather, this limit is due to the fact that the interfacial impedance is purely capacitive (imaginary) at high frequencies and the overall impedance is distributed throughout the porous electrode. Equations 51 and 52 dictate how the interfacial impedance at high frequencies is distributed throughout the porous electrode, subject to the ohmic resistance of the solid and solution. Since the square root of a complex number has a phase angle equal to one-half the phase angle of the argument, the impedance, which is purely capacitive (phase angle 90°) in the high-frequency limit, yields a distributed impedance with a 45° line. Indeed, the entire RC interfacial impedance, which is a semicircle for the single particle, yields a "squashed" semicricle when the impedance is distributed according to the ohmic drop in the porous electrode.

Also shown in Fig. 14 is a plot of the impedance for a porous electrode with the same particle properties in Table III but with infinite solid-phase and solution-phase conductivities ($\kappa, \sigma \to \infty$). When there is no ohmic drop in the solid phase or in solution, the electrode is uniformly accessible. The distributed nature of the impedance results in just an enhancement of the available surface area. Rather than passing current through only a single particle, current passes through all of the particles in the porous electrode without any additional ohmic drop. Clearly the ohmic drop in the solution phase for the system described by the values in Tables III and IV greatly affects the overall impedance of the porous electrode, increasing its magnitude and decreasing its phase angle. The porous electrode can also be made more accessible by making it very thin. Constructing a very thin electrode can be useful in reducing the ohmic effects and recapturing the expression for the impedance given for a single particle, with an enhancement of the available surface area. In this way, one might be able to use the results of Eq. 27 to determine solid-phase diffusion coefficients.

It is clear that the breadth of the particle-size distribution affects the solid-phase diffusion impedance except in its high-frequency limit, as described by Eq. 27. This limiting case for diffusion is independent of the particle-size distribution as long as a is known. It could be used to determine the diffusion coefficient in the solid, provided that it is possible to resolve the high-frequency diffusion limit and the interfacial impedance. As shown in Fig. 14 and even in the single-particle simulations in Fig. 10 and 12, there is sometimes incomplete resolution of these two processes, making it difficult to determine the solid-phase diffusion coefficient in this manner. The low-frequency limit yields no useful information about the diffusion coefficient in the solid unless the particle-size distribution is well known.

Conclusions

The impedance response of a single intercalation particle is developed and can provide information about fundamental properties of the charge-transfer, double-layer, and solid-phase diffusion processes. One can also consider the effects of an insulating film and an additional impedance at the external film/solution interface.

When incorporating the admittance of a single particle into a model which describes the response of a porous electrode, one can still determine information about the charge-transfer and double-layer properties of the interface, and about the solid-phase diffusion coefficient D_s. The limiting forms of the solid-phase impedance can provide useful means of plotting the impedance to determine the solid-phase diffusion coefficient D_s, but the limiting form is independent of the particle-size distribution only in the high-frequency limit. Care must be taken to reduce (or to account for properly) the effect of ohmic drop in the porous electrode when making these measurements, and also to avoid the problems of the resolution of the diffusion impedance when there is overlap from the interfacial impedance.

If one wants to try to fit the impedance of a porous electrode over the entire frequency range to try to gather information about the solid-phase diffusion coefficient and the slope of the OCP, detailed information about the particle-size distribution is necessary.

Acknowledgments

This work was funded by a fellowship from the Office of Naval Research. Additional support was received from the Army Research Office, University of Minnesota MURI, and from E. I. DuPont de Nemours.

The University of California, Berkeley, assisted in meeting the publication costs of this article.

References

1. C. Ho, I. D. Raistrick, and R. A. Huggins, *J. Electrochem. Soc.*, **127,** 343 (1980).
2. R. V. Homsy and J. Newman, *J. Electrochem. Soc.*, **121,** 521 (1974).
3. D. A. Scherson and J. Newman, *J. Electrochem. Soc.*, **127,** 110 (1980).
4. B. Tribollet and J. Newman, *J. Electrochem. Soc.*, **130,** 2016 (1983).
5. B. Tribollet and J. Newman, *J. Electrochem. Soc.*, **131,** 2780 (1984).
6. J. S. Newman and C. W. Tobias, *J. Electrochem. Soc.*, **109,** 1183 (1962).
7. A. M. Johnson and J. Newman, *J. Electrochem. Soc.*, **118,** 510 (1971).
8. J. Newman and W. Tiedemann, *AIChE J.*, **21,** 25 (1975).
9. D. C. Grahame, *J. Electrochem. Soc.*, **99,** 370 (1952).
10. M. Abramowitz and I. A. Stegun, *Handbook of Mathematical Functions*, p. 82, Dover Publications, Inc., New York (1972).
11. R. D. Armstrong, *J. Electroanal. Chem.*, **198 (**1986).
12. T. Jacobsen and K. West, *Electrochim. Acta*, **40** (1995).
13. J. S. Newman, *Electrochemical Systems*, 2nd ed., p. 468, Prentice-Hall, Inc., Englewood Cliffs, NJ (1991).
14. I. J. Ong and J. Newman, *J. Electrochem. Soc.*, **146,** 4360 (1999).
15. M. Doyle, A. S. Gozdz, J. Meyers, and J. Newman, in *Advances in Mathematical Modeling and Simulation of Electrochemical Processes*, J. Van Zee, T. Fuller, P. C. Foller, and F. Hine, Editors, PV 98-10, p. 46, The Electrochemical Society, Pennington, NJ (1998).
16. M. Doyle, J. Meyers, and J. Newman, *J. Electrochem. Soc.*, **147,** 99 (2000).